




# Transplanted Human Multipotent Stromal Cells Reduce Acute Tongue Fibrosis in Rats

Andrew M. Vahabzadeh-Hagh, MD ; Alexander N. Goel ; John W. Frederick, MD; Gerald S. Berke, MD; Jennifer L. Long, MD, PhD 

**Background:** Tongue fibrosis resulting from head and neck cancer, surgery, radiation, chemotherapy, or a combination thereof devastates one's quality of life. Therapeutic options are limited. Here we investigate human bone marrow-derived multipotent stromal cells (MSC) as a novel injectable treatment for post-injury tongue fibrosis.

**Methods:** MSCs were grown in culture. Eighteen athymic rats underwent unilateral partial glossectomy. After two weeks for scar formation, a single injection was performed in the tongue scar. Three treatment groups were studied: low and high concentration MSC, and control media injection. Tongues were harvested for evaluation at three weeks post-treatment.

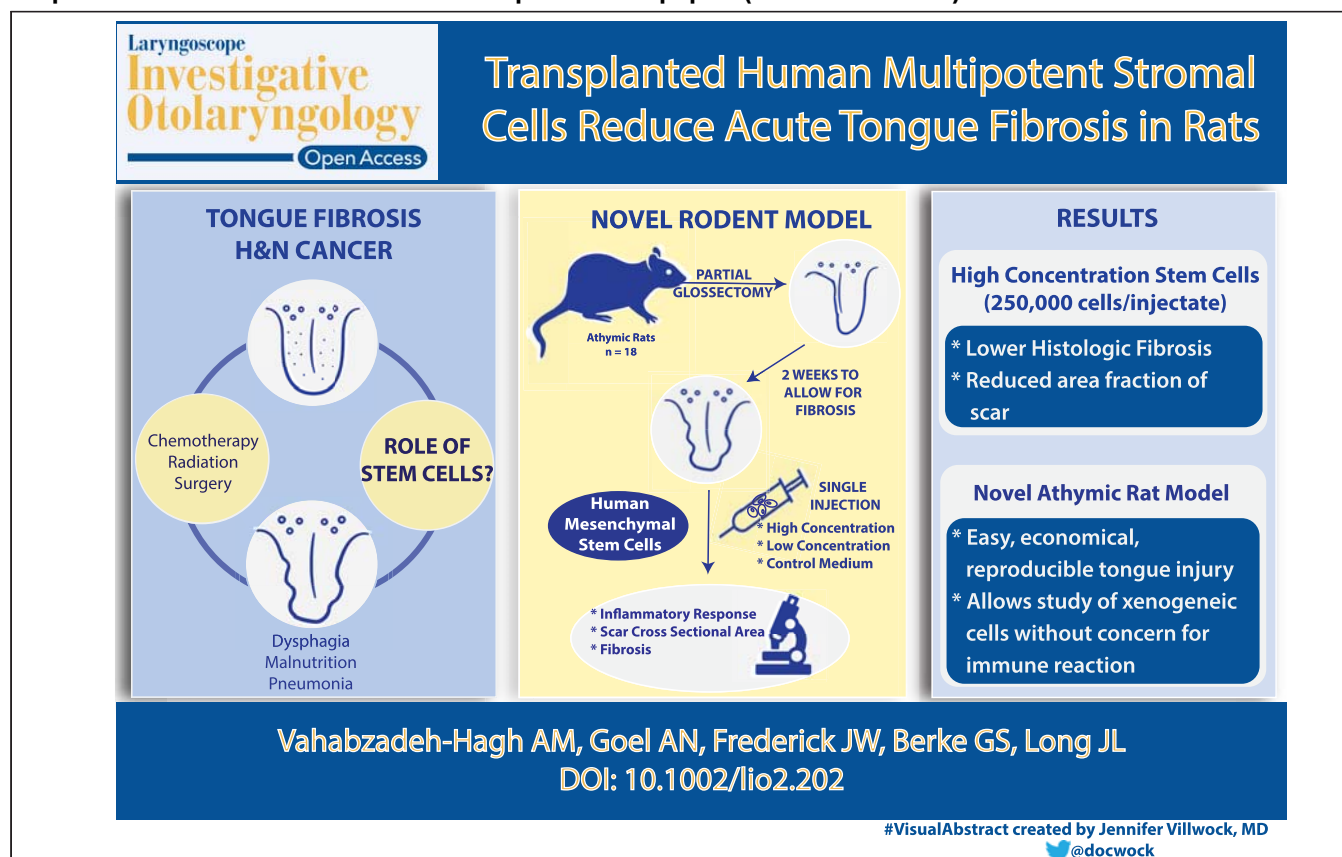
**Results:** Dense fibrosis was achieved in control animals at five weeks. High concentration MSC reduced cross sectional scar burden ( $P = .007$ ) and pathologic score for inflammation and fibrosis.

**Conclusion:** This study establishes the feasibility of a novel rodent tongue fibrosis model, and begins to assess the utility of human MSCs to reduce scar burden.

**Key Words:** Tongue fibrosis, partial glossectomy, rodent, dysphagia, human multipotent stromal cells.

**Level of Evidence:** N/a

A Special Visual Abstract has been developed for this paper. (Visual Abstract 1)



## INTRODUCTION

The tongue is a versatile and critical organ. It is instrumental in speech articulation, deglutition, and airway protection. Structural and therefore functional integrity of the tongue may be compromised in head and neck cancer treatment. Surgery, radiation therapy, and chemotherapy all contribute to denervation, fibrosis, and wasting of the lingual muscles. Specifically, weakness and fibrosis of the base of tongue may lead to a disabling dysphagia. Clinical consequences of severe dysphagia can be devastating and include malnutrition, feeding tube dependence, pneumonia, and death.<sup>1,2</sup>

Current therapies are highly limited and often rely primarily on swallow rehabilitative exercises. Among these, isometric lingual strengthening specifically targets tongue strength and mobility as a way to improve oropharyngeal swallow. These lingual resistance exercises have shown a positive impact on young and older healthy adults as well as those with neurologic impairment such as stroke.<sup>3</sup> However, tongue strength and quality of life in head and neck cancer patients have failed to improve with these exercises.<sup>4</sup> Perhaps the success of these strengthening exercises relies upon normal tongue muscular anatomy, which is deficient in head and neck cancer patients. Innovative new therapies that target structural changes in the damaged tongue may provide benefit in these patients.

Cell-based therapy for the base of tongue is a novel approach to treating atrophy and fibrosis. Limited animal models of tongue function or structure have been published. Lever et al. developed a reliable model of presbyphagia characterized by slowed swallow across all stages in aging B6 mice (18 to 21 months old).<sup>5</sup> Virgin et al. described a reversible equine dysphagia model through the administration of local anesthesia into the guttural pouch to evaluate surgical treatments of dysphagia.<sup>6</sup> Plowman et al. developed a partially denervated ovine tongue model in which the hypoglossal nerves were compressed using cuff electrodes. The electrodes could then be used for later tongue stimulation with measurements of lingual contractile force. Using this model, tongue strength improved after injection of myoblasts from skeletal muscle in one sheep; a second sheep could not be tested.<sup>7</sup> Luxamechanporn et al. developed a rat tongue reconstruction model with a mucosa-sparing hemiglossectomy pocket. These pockets were then filled with either collagen or myoblast/collagen constructs. Improved muscle regeneration and less scar contracture occurred after six weeks with the myoblast/collagen constructs.<sup>8</sup>

---

From the Department of Head and Neck Surgery, UCLA David Geffen School of Medicine (A.N.G., J.W.F., G.S.B., J.L.L.), Los Angeles, California, U.S.A.; Department of Surgery, Division of Otolaryngology UC San Diego Health (A.M.V.), La Jolla, CA; Research Service (J.L.L.), Greater Los Angeles VA Healthcare System, Los Angeles, California, U.S.A.

Editor's Note: This Manuscript was accepted for publication 1 July 2018.

This material is based upon work supported by the Department of Veteran Affairs, Veterans Health Administration, Office of Research and Development, Biomedical Laboratory Research and Development (Jennifer Long), VA Career Development Award IK2BX001944 (Jennifer Long).

Send correspondence to Jennifer L. Long, 10833 Le Conte Ave, 62-132, Los Angeles, CA 90095. Email: JLong@mednet.ucla.edu

DOI: 10.1002/lto.2202

While these studies are promising, a drawback of myoblast therapy is the difficulty in expanding these committed cells to an adequate therapeutic number. Adult multipotent stromal cells are more accessible and may offer greater benefit than myoblasts by acting in other pathways to reduce fibrosis, improve angiogenesis, and promote proliferation through pro-survival and anti-apoptotic effects.<sup>9</sup> While they have not been used in the tongue, MSCs have been applied to other muscle tissues. Shudo et al. introduced co-cultured functional skeletal myoblasts and human adipose-derived MSCs into a rodent myocardial infarction model. Their work demonstrated increased levels of the paracrine factors rat hepatocyte growth factor and vascular endothelial growth factor. Eight weeks later the greatest functional improvement occurred in this co-cultured treatment group.<sup>9</sup> Okura et al. used adipose-derived MSC patches transplanted onto a nude rat myocardial infarction model. They found rescue and maintenance of myocardial function as well as engraftment onto scarred myocardium by implanted cells differentiated into cardiomyoblast-like cells.<sup>10</sup> Chen et al. studied bone marrow-derived MSC in a canine urethral defect model. They transplanted decellularized human amniotic scaffolds seeded with allogeneic bone marrow MSC and endothelial progenitor cells and found post-treatment unhindered urination and adequate urethral caliber.<sup>11</sup> The potential clinical applications of MSC in muscle tissues are thus widespread.

Here we develop a new rodent model of tongue scar and fibrosis which we refer to as the quadrant glossectomy model. We demonstrate its ease of application, and robust and consistent results. Using this model we investigate the application of human bone marrow-derived MSC in low- (L) and high-dose (H) administrations. Influence on tongue inflammation, fibrosis, and mass is measured. We hypothesized that MSC would reduce the emergence of non-functional scar tissue. Experimental schema is shown in Figure 1. The timeline was chosen based on the standard wound healing sequence of hemostasis, inflammation, proliferation, and tissue remodeling, which does proceed more rapidly in rats than in humans.<sup>12</sup> Very early wound manipulation (within 48 hours) can shift the growth factor and cell infiltration profile, and produce overly optimistic results that may not be relevant to most clinical scenarios.<sup>13</sup> The two-week time-point was therefore chosen for intervention because that early pathway-determining window has passed, and the tissue remodeling phase is underway. By five weeks, extracellular matrix remodeling slows, yet continues for up to three months. Focusing the intervention between weeks two and five thus studies MSC influence during the critical phase of matrix metalloproteinase action, collagen deposition, and fibroblast and macrophage activity.

## MATERIALS AND METHODS

### *MSC Source and Culture*

Human bone marrow-derived MSCs were commercially purchased in two separate lots (Life Technologies Corporation, San Diego, California, U.S.A.).<sup>14</sup> For quality control, each lot was phenotypically confirmed with flow cytometry for standard markers and by multi-potency on directed differentiation assay. MSCs were

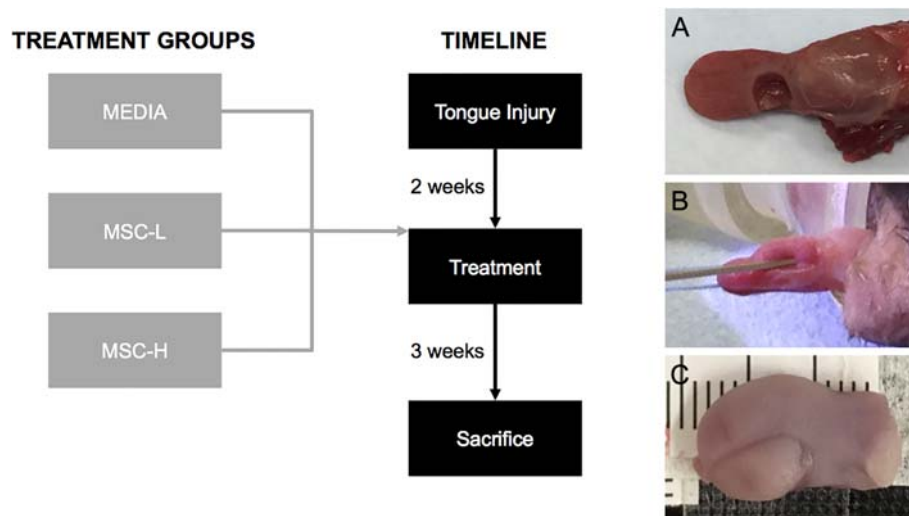


Fig. 1. **Experimental design and partial glossectomy model.** Flow diagram depicts different treatment groups, time of injury, treatment, and sacrifice. Groups include: Media, Bone marrow-derived multipotent stromal cells low concentration (MSC-L), and Bone marrow-derived multipotent stromal cells high concentration (MSC-H). (A) demonstrates total glossectomy specimen with fresh partial glossectomy defect created using a 4 mm dermal punch. (B) 25-gauge needle used to inject treatment solution into center of tongue scar 2 weeks after injury. (C) 5-week scar following quadrant glossectomy resulting in ipsilateral tongue contracture and fissure seen in the coronal plane.

cultured with DMEM/F12 basal medium plus 10% fetal bovine serum (FBS) and 1% antimycotic/streptomycin solution. Cells were harvested for tongue treatment after passage 2. The desired number of cells for treatment were resuspended in 300 microliters of culture medium, namely the 10% FBS and 1% antimycotic/streptomycin in DMEM. Low concentration group (MSC-L) received 70,000 cells per injectate and the high concentration group (MSC-H) received 250,000 cells per injectate. Cell number range was chosen based on prior studies of MSC for skeletal muscle repair in rat models which administered cells in the range of  $10^4$  to  $10^6$  cells/kg.<sup>15,16</sup> Control group received 300 microliters of culture medium alone.

### Partial Glossectomy Model

This study was performed in accordance with the PHS Policy on Humane Care and Use of Laboratory Animals, the NIH *Guide for the Care and Use of Laboratory Animals*, and the Animal Welfare Act (7 U.S.C. et seq.); the animal use protocol was approved by the local Institutional Animal Care and Use Committee. All measures were taken to minimize pain and discomfort of subject animals throughout the experiment. Eighteen Rowett nude (Rnu) rats were randomized into one of three groups: Media alone (n = 6), Multipotent stromal cells in low (MSC-L, n = 6) and high (MSC-H, n = 6) concentrations. At 40 days of age and  $125 \pm 10$  grams of weight, all animals underwent a partial glossectomy. The rats were anesthetized with isoflurane, tongue withdrawn and retracted with a 4-0 silk suture, and a 4-mm dermal punch used to excise approximately 25% of the tongue (quadrant glossectomy), just anterior to the circumvallate papillae on the left side leaving the ventral tongue mucosa intact. Silver nitrate chemical cautery was used for hemostasis. At the site of injury for local analgesia, 2 mg/kg of plain marcaine was injected submucosal. The rats were provided a soft diet postoperatively and enrofloxacin was diluted to a concentration of 0.5 mg/mL in their drinking water for five days postoperatively. Animals were weighed regularly. Formation of scar tissue was then observed over the subsequent two weeks. Figure 1A, 1B, and 1C demonstrates the partial glossectomy model, treatment injection, and resultant gross tongue scar, respectively.

### Cell Injection and Follow-Up

Two weeks following injury, the rats were anesthetized again, tongue withdrawn, and 300 microliters of the group-specific treatment solution was injected submucosally in the center of the maturing scar. Three weeks later the rats were euthanized and the tongues were harvested, transected just posterior to the circumvallate papillae, measured, weighed, and formalin fixed for tissue processing. Tongue harvest was performed using a transcranial total glossectomy technique. A standardized 1 cm long segment of tongue was excised centered at the tongue scar with posterior limit at the circumvallate papillae (Fig. 1C). Volumes of the excised tongue were computed by approximating the tongue as an ellipsoid, where the volume is equal to  $4/3\pi(abc)$ ; "a", "b", and "c" equal to the lengths of the semi-principal axes.<sup>17</sup> Inter-group statistical analysis was performed using one-way analysis of variance (ANOVA) followed by a post-hoc multiple comparisons Fisher's least significant difference (LSD) test with a level of statistical significance set at  $P < .05$  (IBM SPSS Statistics, v24).

### Post-Mortem Histology and Immunohistochemistry

Hematoxylin and eosin (H&E) stain and immunohistochemical staining for CD3, a lymphocyte marker, were used to assess tongue fibrosis, inflammation, the fraction of cross-sectional area encompassed by scar at the center of the glossectomy defect, lymphocyte density, and vascularity of the scarred tongue. A board-certified pathologist performed a standardized blinded assessment of the degrees of inflammation and fibrosis rated on a pathologic score from 0, no inflammation or fibrosis, to 3, severe inflammation or fibrosis.

Scar extent was evaluated by measuring the fraction of cross-sectional area encompassed by scar, measured at the center of the glossectomy defect. Two independent blinded reviewers circumscribed the scar area on H&E stains that was then quantified using ImageJ software (ImageJ 1.42q, Wayne Rasband, National Institutes of Health, USA). Scar area can easily be defined by the basophilic predominance on H&E stain, with abundant nuclei, dense stroma, and complete lack of the characteristic eosinophilic muscle fibers of the normal tongue. Blood vessels were counted by H&E

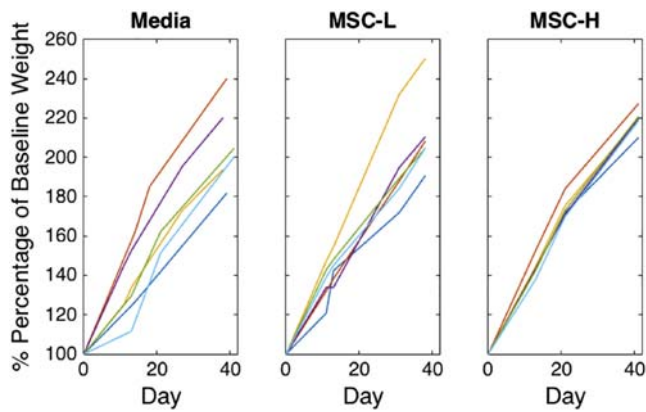


Fig. 2. **Rat weight.** Rat weights throughout the experiment (Days) are expressed as a percentage of their baseline weight (100%) at the start of experimentation. Each subgraph corresponds to a different treatment group as reflected by the title. All treatment groups demonstrate weight gain throughout the experiment.

stained slides identifying red blood cells within a lumen on two fields at 20x. Number of CD3 positive cells was counted per 20x field (rabbit polyclonal anti-CD3 antibody, DAKO, A0452).

Masson's trichrome staining was performed to assess collagen deposition. A group-blinded reviewer circumscribed scar area on 4x images of the tongue scar that were stained using Masson's trichrome method. Image J software was then used to count blue pixels indicating collagen.

Hydroxyproline content was also measured as an indicator of total collagen. Formalin-fixed, paraffin-embedded tissue shavings were collected at the time of tissue sectioning. Paraffin was

dissolved by xylene soaking for ten minutes twice, followed by ethanol dehydration to 70% ethanol. Samples were dried and weighed. Acid hydrolysis in 12 M HCl for three hours at 120 C released free amino acids. A sample of the supernatant was assayed using Sigma hydroxyproline assay kit based on chloramine T/DMAB reaction (Catalog # MAK008, Sigma-Aldrich, St. Louis, MO, USA). Results are presented as hydroxyproline content normalized to dry mass and are averaged among the samples of each group.

Terminal deoxynucleotidyl transferase dUTP nick-end labeling (TUNEL) assay for apoptotic cells was performed using terminal deoxynucleotidyl transferase (TdT) labeling of paraffin-embedded, formalin-fixed slides (Trevigen #4810, Gaithersburg, MD, USA). Images were taken at 4x, and examined with ImageJ. Scar area was circumscribed, and the TdT-positive cell count density was quantified within the scar area.

## RESULTS

Eighteen rats underwent quadrant partial glossectomy, and follow-up injection of either MSC or growth media alone after two weeks. All rats survived until harvest at five weeks, and gained weight. Rat weight progression was used as a surrogate for functional recovery, dietary intake, and overall tolerance of the quadrant glossectomy model. Figure 2 demonstrates the positive progression of weight for each rat in each treatment group over time. Weight is represented as a percentage of the baseline weight. All rats in all treatment groups showed weight gain over time, achieving 206% to 230% of their baseline weight on average by five weeks and matching

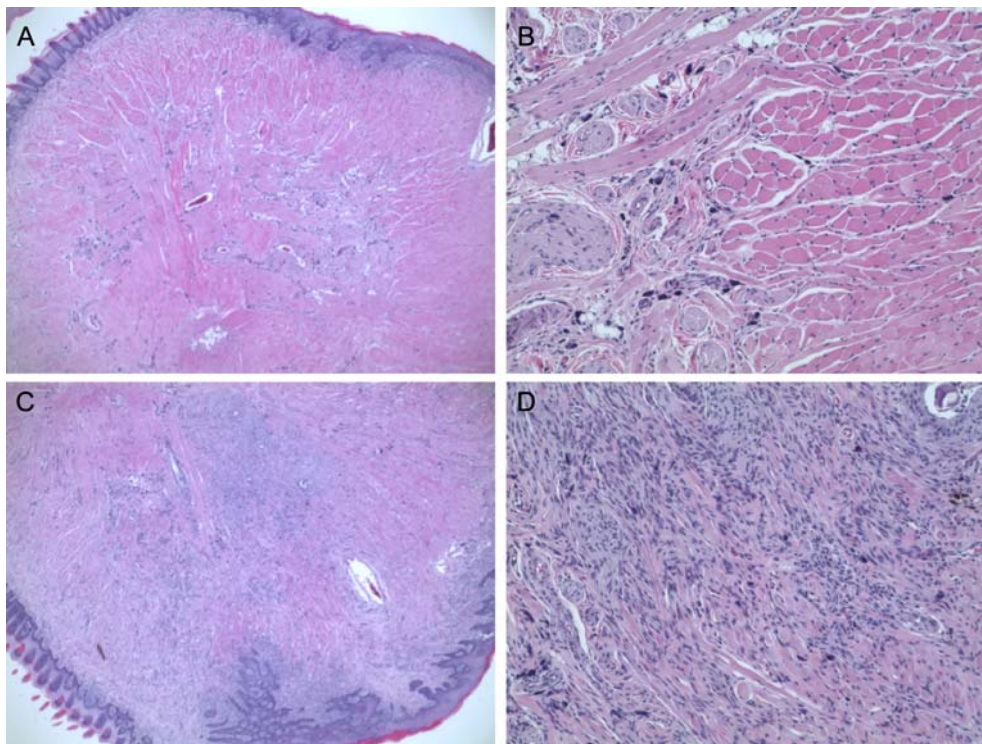


Fig. 3. **Hematoxylin and Eosin stain of tongue scar at 5 weeks.** Axial cuts, perpendicular to the long axis of the tongue demonstrating (A) low power (4x) and (B) high power (20x) H&E stain of the contralateral uninjured hemi tongue. (C) Low power (4x) and (D) high power (20x) H&E stain of the ipsilateral injured hemi tongue. (C) and (D) illustrate dense stromal fibrosis, lymphocytic infiltrate, and loss of a significant portion of the intrinsic muscular architecture of the tongue. (A) and (B) show well maintained histological architecture of the tongue with preservation of intrinsic vertical, transverse, and longitudinal muscle fibers.

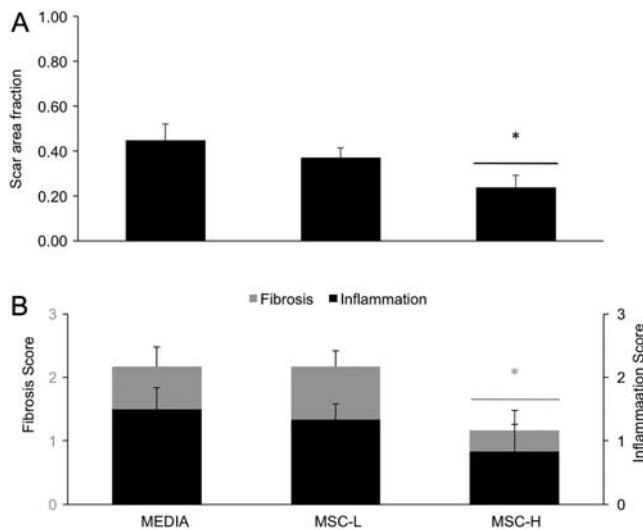


Fig. 4. **Tongue scar area fraction and degrees of fibrosis and inflammation.** (A) **Scar area fraction.** Area of scar was measured on H&E-stained sections and divided by total area to produce the scar area fraction. Significant intergroup difference was achieved,  $P = .023$ . Post-hoc multiple comparisons showed MSC-H group with significantly less scar area percentage ( $P = .007$ ) highlighted by the asterisk. Error bars are equal to the standard error of the mean (SEM). (B) **Pathologic ratings for fibrosis and inflammation.** Each section was rated with semi-quantitative scores for fibrosis (on primary vertical axis) and inflammation (on secondary vertical axis) and averaged for each group. Intergroup difference for fibrosis was significant,  $P = .027$ , with post-hoc multiple comparisons confirming less fibrosis in the MSC-H treatment group ( $P = .019$ ).

the average growth chart for this strain (CrI:NIH-Foxn1<sup>rn</sup>, Charles River Laboratories International, Inc.).

The gross metrics (weight and volume) of the excised tongues five weeks post-quadrant glossectomy failed to demonstrate significant intergroup differences. Average tongue volumes were 204, 194, and 244 mm<sup>3</sup> for Media, MSC-L, and MSC-H treated groups, respectively. Average tongue weights were 288, 269, and 321 mg for Media, MSC-L, and MSC-H treated groups, respectively. At two weeks post-quadrant glossectomy, the defect was reduced to a thickened fissure. By five weeks, a robust histological scar was appreciated. The scar is characterized by dense stromal fibrosis, lymphocytic infiltrate, and a loss of the intrinsic muscular architecture of the tongue as shown in a scarred, untreated tongue in Figure 3. Notably, by five weeks, the defect was filled or largely replaced with scar tissue with a well-formed re-mucosalized surface.

On H&E stains, a significant decrease in scar area as a fraction of the total cross-sectional area of the tongue was found for the MSC-H treated group in comparison to the Media control ( $P = .007$ ) as shown in Figure 4A. Scores from the blinded reviewers were combined and presented as an average score. Interrater bias was near zero (bias = -0.007) and the Pearson correlation coefficient was 0.97. Fibrotic and inflammatory responses observed in histologic sections were rated by a board-certified pathologist using semi-quantitative scales. Pathologic score ranged from zero, no inflammation or fibrosis to three, severe inflammation or fibrosis. Intergroup difference for fibrosis was significant,  $P = .027$ , with post-hoc multiple comparisons confirming lower fibrosis score in the MSC-H

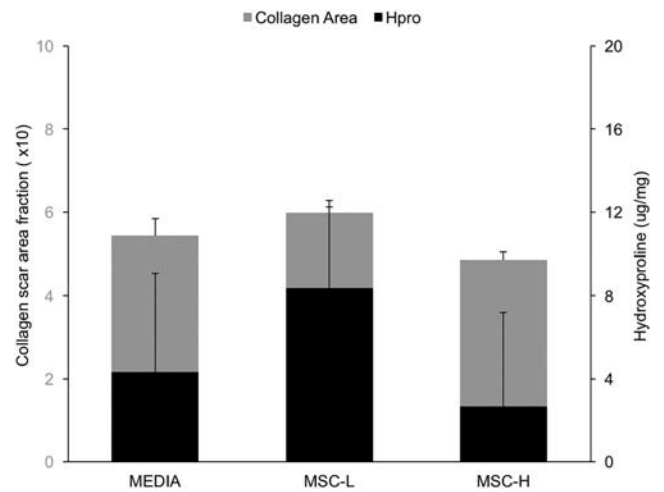


Fig. 5. **Collagen scar area fraction and hydroxyproline content.** Trichrome-stained sections were photographed on 4x views at the center of the tongue scar. Blue pixels were quantified as a histologic measure of collagen, and presented as a fraction of total pixels (primary vertical axis). Quantitative hydroxyproline content was measured in homogenized tissue specimens and normalized to dry weight (secondary vertical axis). Intergroup difference for histologic collagen area fraction was significant,  $P = .028$  but post-hoc tests failed to demonstrate significance for either treatment group compared to the control. Intergroup difference for hydroxyproline content was significant,  $P = .029$ , with post-hoc multiple comparisons demonstrating this difference driven by higher content in the MSC-L treatment group ( $P = .056$ ). Error bars are equal to the standard error of the mean (SEM).

treatment group ( $P = .019$ ) (Fig. 4B). Inflammation score did not differ statistically. Also, the number of CD3-positive cells (a marker of T lymphocytes) did not differ among groups (7.5, 7.0, and 4.4 cells per 40x field in media, MSC-L, and MSC-H groups, respectively).

On Masson's trichrome stains, overall density of collagen area as determined by image pixel analysis showed significant intergroup differences ( $P = .028$ ) but post-hoc tests did not reach significance for either treatment group (Fig. 5). Intergroup difference for hydroxyproline content was significant,  $P = .029$ , with post-hoc multiple comparisons showing higher content in the MSC-L treatment group ( $P = .056$ ) (Fig. 5). The significance of this finding is unclear and did not mirror the other semi-quantitative measures of collagen deposition and fibrosis.

Presence of erythrocytes allowed easy identification of blood vessels in the region of the mature tongue scar. There was no intergroup difference for vessel count among treatment groups (45, 38, and 42 cells per 20x field in media, MSC-L, and MSC-H groups, respectively). Also, TUNEL staining for apoptotic cells within the scar area showed that MSC-treated tongues did not differ from controls (1.9, 1.9, and 1.7 cells per section in media, MSC-L, and MSC-H groups, respectively).

## DISCUSSION

Treatment of advanced head and neck cancer often involves a multidisciplinary and multimodal treatment approach. Surgery, radiation, chemotherapy, or a combination thereof, even though implemented with the goal of

curative yet functionally preserving therapy, often results in debilitating dysphagia. Oropharyngeal function relies on musculature extending from the skull base to at least the hyoid bone. In treatment of advanced stage head and neck cancer, this important region is almost inevitably in the center of the treatment field. Dysphagia may result immediately following surgical therapy or as soon as four to five weeks following radiation therapy.<sup>18,19</sup> Posttreatment dysphagia results in dietary changes, prolonged meal times, non-oral dietary dependence, anorexia, and malnutrition. Furthermore, it is estimated that 36% to 94% of head and neck cancer patients will have aspiration which can be life threatening.<sup>8,18,20–22</sup> Current therapies, such as lingual strengthening exercises, have failed to demonstrate significant improvement in tongue strength or quality of life in head and neck cancer patients. While these exercises may improve functional dynamic motion of the tongue, they do little to reverse fibrotic changes which may serve as a critical barrier to their efficacy. Mesenchymal stem cell therapy aims to reduce tongue atrophy and fibrosis and represents a promising approach to restore structure and function to the damaged tongue.

Here we evaluate the effect of multipotent stromal cells in a tongue scar model that mimics posttreatment oral and base of tongue cancers. A previously reported ovine tongue model induced tongue weakness through partial denervation of the hypoglossal nerve.<sup>3</sup> While this innovative model is relevant to dysphagia from tongue atrophy, such as occurs in neurodegenerative disorders, head and neck cancer treatment produces tongue fibrosis, with stiff collagen replacing some of the muscle bulk. Another previously published rat tongue model implanted three-dimensional constructs within a mucosal pocket at the time of mucosa-sparing partial glossectomy.<sup>8,23,24</sup> Such a model does not replicate the surgical resection of tongue cancer, which results in defects of both mucosa and underlying muscle. Also, immediate cell treatment at the time of a cancer resection is not compatible with the primary goal of cancer extirpation. Here, we implement a true quadrant partial glossectomy (including mucosa) and allow time for the tongue scar to begin maturation before intervening. This novel but simple model maximizes the imparted defect and evokes a robust fibrotic and inflammatory response (Fig. 3). Yet our animal subjects demonstrate great tolerance of this defect as evidenced by the positive normal growth curve for all treatment groups (Fig. 2). As such, this model provides a severe enough injury to mimic posttreatment advanced stage oral and base of tongue cancers, while avoiding potential nutritional confounders and any study dropouts. Furthermore, this model is easy to perform, financially and temporally economical, and provides a very reproducible tongue injury. Using athymic rats allows study of xenogeneic cells without concern of immune reaction, to best replicate an autologous cell transplant model.

In this model, we begin to assess the influence of mesenchymal stromal cells on tongue fibrosis. MSCs can be sourced from multiple tissues, and are defined by their fibroblastoid phenotype, adherence to plastic, characteristic signature of cell surface molecules, and trilineage mesodermal differentiation capacity *in vitro*.<sup>25</sup> MSCs

have developed an extensive safety profile in human clinical trials and are easy to harvest from adults and expand in culture. MSCs are capable of differentiating to muscle cells *in vitro*,<sup>26,27</sup> but they have not clearly become myoblastic *in vivo* simply by introducing them into muscle.<sup>28</sup> Rather, the supportive actions of the MSC secretome distinguish them from myoblasts and prompt their use in this application. Specifically, MSCs are selected for their pro-survival paracrine effects that induce fibroblast migration and their immunomodulatory actions that reduce the inflammatory cascade.<sup>29</sup>

The pharmacodynamics of MSC therapy is far from understood and prior reports have used a wide range of administered cells. Studies in myocardial infarction animal models, for example, have demonstrated benefit with doses ranging from  $1 \times 10^5$  cells/kg<sup>30</sup> to  $1 \times 10^7$  cells/kg<sup>31</sup> and there is evidence both for dose-dependent<sup>32</sup> and dose-independent responses.<sup>33</sup> As such, this work aimed to define an appropriate cell dose range by testing low and high concentrations of administered MSCs. The high concentration group (MSC-H) demonstrated benefit relative to controls across several measures, whereas the low concentration group (MSC-L) did not differ significantly from controls. Overall, both doses were well tolerated in these athymic, T-cell deficient rats without any signs of rejection or intolerance. High-dose MSC (MSC-H) significantly reduced the area fraction of scar on H&E stains (Fig. 4A) with reduced histologic fibrosis score (Fig. 4B).

While fibrosis and scar fraction were reduced in the MSC-H group, a corresponding reduction in collagen was not observed. This may be due to evolving collagen content at 35 days post-glossectomy; collagen deposition has been shown to steadily increase up to 70 days post-injury in the natural course of rat wound healing.<sup>34</sup> It is possible that a longer study would amplify any group differences in collagen. Additionally, given that the healthy tongue contains a significant amount of collagenous fibrous tissue between muscle fiber bundles, we hypothesize that overall collagen content in the tongue may be a less meaningful metric of fibrotic changes than histologic analysis in the area of injury itself. Furthermore, Masson's trichrome stain highlights only the collagen, while excluding other features of the scar such as fibroblasts and fibronectin. These additional components of scar may contribute to the discrepancy between collagen area and scar area.

Potential mechanisms for reduced scar area and fibrosis with MSC treatment were explored in this model. Fibrosis is often precipitated by inflammation, but semi-quantitative inflammation score did not reach statistical significance in this model ( $P = .08$ ). Although T cell maturation is impaired in these athymic rats (as confirmed by unchanged CD3+ cell counts), innate immunity remains intact. More sensitive evaluation methods for early-responding innate inflammatory cells would be worthwhile. Neither MSC group demonstrated an appreciable change in vascularity, arguing against angiogenesis as an independent mechanism. Apoptotic cell counts did not differ between MSC-treated tongues and controls; apoptosis was inversely correlated with fibrosis in a mouse lung fibrosis model.<sup>35</sup> These data argue against a mechanism of fibroblast apoptosis producing reduced fibrosis in this

acute tongue injury model. Further study focusing on MSC-derived cytokines is merited and planned.<sup>15</sup>

This work establishes a new rodent quadrant partial glossectomy model as a realistic tool for studying tongue fibrosis after head and neck cancer treatment. Our outcome metrics demonstrate reduced scar formation with bone marrow-derived multi-potent stromal cell injection administered in a high cellular concentration, but not in a low cellular concentration. Mechanistic exploration suggests that anti-fibrotic actions may contribute to this effect. This model can enable further investigation of pharmaceutical or cell-based therapies for anatomic and functional tongue regeneration.

## BIBLIOGRAPHY

1. Falsetti P, Acciai C, Palilla R, Bosi M, Carpinteri F, Zingarelli A, Pedace C, Lenzi L Oropharyngeal dysphagia after stroke: incidence, diagnosis, and clinical predictors in patients admitted to a neurorehabilitation unit. *J Stroke Cerebrovasc Dis* 2009;18:329–335.
2. Nguyen NP, Moltz CC, Frank C, Vos P, Smith HJ, Karlsson U, Dutta S, Midyett FA, Barloon J, Sallah S Dysphagia following chemoradiation for locally advanced head and neck cancer. *Ann Oncol* 2004;15:383–388.
3. Easterling C. 25 Years of Dysphagia Rehabilitation: What have we done, what are we doing, and where are we going? *Dysphagia* 2017;32:50–54.
4. Lazarus CL, Husaini H, Falciglia D, DeLaure M, Branski RC, Kraus D, Lee N, Ho M, Ganz C, Smith B, Sanfilippo N Effects of exercise on swallowing and tongue strength in patients with oral and oropharyngeal cancer treated with primary radiotherapy with or without chemotherapy. *Int J Oral Maxillofac Surg* 2014;43:523–530.
5. Lever TE, Brooks RT, Thombs LA, Littrell LL, Harris RA, Allen MJ, Kadosh MD, Robbins KL Videofluoroscopic validation of a translational murine model of presbyphagia. *Dysphagia* 2015;30:328–342.
6. Virgin JE, Holcombe SJ, Caron JP, Cheetham J, Kurtz KA, Roessner HA, Ducharme NG, Hauptman JG, Nelson NC Laryngeal advancement surgery improves swallowing function in a reversible equine dysphagia model. *Equine Vet J* 2016;48:362–367.
7. Plowman EK, Bijangi-Vishehsaraei K, Halum S, Cates D, Hanenberg H, Domer AS, Nolita JA, Belafsky PC Autologous myoblasts attenuate atrophy and improve tongue force in a denervated tongue model: a pilot study. *Laryngoscope* 2014;124:E20–E26.
8. Luxameechanporn T, Hadlock T, Shyu J, Cowan D, Faquin W, Varvares M. Successful myoblast transplantation in rat tongue reconstruction. *Head Neck* 2006;28:517–524.
9. Shudo Y, Miyagawa S, Ohkura H, Fukushima S, Saito A, Shiozaki M, Kawaguchi N, Matsuura N, Shimizu T, Okano T, Matsuyama A, Sawa Y Addition of mesenchymal stem cells enhances the therapeutic effects of skeletal myoblast cell-sheet transplantation in a rat ischemic cardiomyopathy model. *Tissue Eng Part A* 2014;20:728–739.
10. Okura H, Matsuyama A, Lee CM, Saga A, Kakuta-Yamamoto A, Nagao A, Sougawa N, Sekiya N, Takekita K, Shudo Y, Miyagawa S, Komoda H, Okano T, Sawa Y Cardiomyoblast-like cells differentiated from human adipose tissue-derived mesenchymal stem cells improve left ventricular dysfunction and survival in a rat myocardial infarction model. *Tissue Eng Part C Methods* 2010;16:417–425.
11. Chen C, Zheng S, Zhang X, Dai P, Gao Y, Nan L, Zhang Y Transplantation of amniotic scaffold seeded mesenchymal stem cells and/or endothelial progenitor cells from bone marrow to efficiently repair 3-cm circumferential urethral defect in model dogs. *Tissue Eng Part A* 2018;24:47–56.
12. Pence BD, Woods JA. Exercise, obesity, and cutaneous wound healing: evidence from rodent and human studies. *Adv Wound Care (New Rochelle)* 2014;3:71–79.
13. Ferguson MW, O’Kane S. Scar-free healing: from embryonic mechanisms to adult therapeutic intervention. *Philos Trans R Soc Lond B Biol Sci* 2004;359:839–850.
14. Chase LG, Yang S, Zachar V, Yang Z, Lakshminpathy U, Bradford J, Boucher SE, Vemuri MC Development and characterization of a clinically compliant xeno-free culture medium in good manufacturing practice for human multipotent mesenchymal stem cells. *Stem Cells Transl Med* 2012;1:750–758.
15. Helal MA, Shaheen NE, Abu Zahra FA. Immunomodulatory capacity of the local mesenchymal stem cells transplantation after severe skeletal muscle injury in female rats. *Immunopharmacol Immunotoxicol* 2016;1–9.
16. Winkler T, von Roth P, Matziolis G, Mehta M, Perka C, Duda GN. Dose-response relationship of mesenchymal stem cell transplantation and functional regeneration after severe skeletal muscle injury in rats. *Tissue Eng Part A* 2009;15:487–492.
17. Mikus JL, Koufman JA, Kilpatrick SE. Fate of liposuctioned and purified autologous fat injections in the canine vocal fold. *Laryngoscope* 1995;105:17–22.
18. Kweon S, Koo BS, Jee S. Change of swallowing in patients with head and neck cancer after concurrent chemoradiotherapy. *Ann Rehabil Med* 2016;40:1100–1107.
19. Murphy BA. Clinical and economic consequences of mucositis induced by chemotherapy and/or radiation therapy. *J Support Oncol* 2007;5(9 Suppl 4):13–21.
20. Caudell JJ, Schaner PE, Meredith RF, Locher JL, Nabell LM, Carroll WR, Magnuson JS, Spencer SA, Bonner JA Factors associated with long-term dysphagia after definitive radiotherapy for locally advanced head-and-neck cancer. *Int J Radiat Oncol Biol Phys* 2009;73:410–415.
21. Eisbruch A, Lyden T, Bradford CR, Dawson LA, Haxer MJ, Miller AE, Teknos TN, Chepeha DB, Hogikyan ND, Terrell JE, Wolf GT Objective assessment of swallowing dysfunction and aspiration after radiation concurrent with chemotherapy for head-and-neck cancer. *Int J Radiat Oncol Biol Phys* 2002;53:23–28.
22. Garcia-Peris P, Paron L, Velasco C, et al. Long-term prevalence of oropharyngeal dysphagia in head and neck cancer patients: Impact on quality of life. *Clin Nutr* 2007;26:710–717.
23. Bunaprasert T, Hadlock T, Marler J, Kobler J., Cowan D., Faquin W., Varvares M. Tissue engineered muscle implantation for tongue reconstruction: a preliminary report. *Laryngoscope* 2003;113:1792–1797.
24. Kim J, Hadlock T, Cheney M, Varvares M, Marler J. Muscle tissue engineering for partial glossectomy defects. *Arch Facial Plast Surg* 2003;5:403–407.
25. Bronckaers A, Hilkens P, Martens W, Gervois P, Ratajczak J, Struys T, Lambrechts I Mesenchymal stem/stromal cells as a pharmacological and therapeutic approach to accelerate angiogenesis. *Pharmacol Ther* 2014;143:181–196.
26. Pittenger MF, Mackay AM, Beck SC, Jaiswal RK, Douglas R, Mosca JD, Moorman MA, Simonetti DW, Craig S, Marshak DR Multilineage potential of adult human mesenchymal stem cells. *Science* 1999;284:143–147.
27. Zuk PA, Zhu M, Ashjian P, de Ugarte DA, Huang JI, Mizuno H, Alfonso ZC, Fraser JK, Benhaim P, Hedrick MH Human adipose tissue is a source of multipotent stem cells. *Mol Biol Cell* 2002;13:4279–4295.
28. Rigol M, Solanes N, Roura S, Roqué M, Novensà L, Dantas AP, Martorell J, Sitges M, Ramirez J, Bayés-Genis A, Heras M Allogeneic adipose stem cell therapy in acute myocardial infarction. *Eur J Clin Invest* 2014;44:83–92.
29. Han ZC, Du WJ, Han ZB, Liang L. New insights into the heterogeneity and functional diversity of human mesenchymal stem cells. *Biomed Mater Eng* 2017;28(s1):S29–S45.
30. Vincentelli A, Wautot F, Juthier F, Fouquet O, Corseaux D, Marechaux S, le Tourneau T, Fabre O, Susen S, van Belle E, Mouquet F, Decoene C, Prat A, Jude B In vivo autologous recellularization of a tissue-engineered heart valve: are bone marrow mesenchymal stem cells the best candidates? *J Thorac Cardiovasc Surg* 2007;134:424–432.
31. Amado LC, Schuleri KH, Saliaris AP, Boyle AJ, Helm R, Oskouei B, Centola M, Eneboe V, Young R, Lima JAC, Lardo AC, Heldman AW, Hare JM Multimodality noninvasive imaging demonstrates in vivo cardiac regeneration after mesenchymal stem cell therapy. *J Am Coll Cardiol* 2006;48:2116–2124.
32. Richardson JD, Bertaso AG, Psaltis PJ, Frost L, Carbone A, Paton S, Nelson AJ, Wong DTL, Worthley MI, Gronthos S, Zannettino ACW, Worthley SG Impact of timing and dose of mesenchymal stromal cell therapy in a preclinical model of acute myocardial infarction. *J Card Fail* 2013;19:342–353.
33. Hamamoto H, Gorman JH. 3rd, Ryan LP, et al. Allogeneic mesenchymal precursor cell therapy to limit remodeling after myocardial infarction: the effect of cell dosage. *Ann Thorac Surg* 2009;87:794–801.
34. Shah M, Foreman DM, Ferguson MW. Control of scarring in adult wounds by neutralising antibody to transforming growth factor beta. *Lancet* 1992;339:213–214.
35. Hecker L, Logsdon NJ, Kurundkar D, et al. Reversal of persistent fibrosis in aging by targeting Nox4-Nrf2 redox imbalance. *Sci Transl Med* 2014;6:231ra47.